MTLA 38 (2024) 102277

Contents lists available at ScienceDirect

Materialia

journal homepage: www.elsevier.com/locate/mtla

Investigation of kinetics of passive layer formation on various microstructures in thermo-mechanically treated steel in simulated concrete pore solution

Gisoo Daviran [a,*], S. M. Ali Seyed Mahmoud [b], Surya R. Kalidindi [c], Amir Poursaee [d]

[a] Glenn Department of Civil Engineering, Clemson University, Clemson, SC, USA
[b] George W. Woodruff School of Mechanical Engineering, Georgia Institute of Technology, Atlanta, GA, USA
[c] George W. Woodruff School of Mechanical Engineering, School of Computational Science and Engineering, School of Materials Science and Engineering, Georgia Institute of Technology, Atlanta, GA, USA
[d] Glenn Department of Civil Engineering, Department of Materials Science and Engineering, Clemson University, Clemson, SC, USA

ARTICLE INFO

Keywords:
Passive layer
SECM
Pearlite
Martensite
Bainite
Concrete
Reinforcing bar

ABSTRACT

Carbon steel bars are critical in steel-reinforced concrete structures, and their corrosion can lead to significant deterioration. This research explored the passive layer formation on different carbon steel microstructures using a high throughput approach. Thermomechanically treated steel bars with three distinct microstructures, i.e., martensite in the outer layer, bainite in the middle, and pearlite in the center, were vertically cut and immersed in the simulated concrete pore solution. Scanning electrochemical microscopy was employed to study the formation of the passive layer, the kinetics of the passivation, and the effective rate constant of the species inside the solution on each microstructure. Results showed that the formation of the passive layer is a time-dependent process, and passivation was influenced by the local microstructure. Martensite demonstrated superior passivation behavior compared to pearlite and bainite.

1. Introduction

The durability of steel-reinforced concrete structures relies heavily on the integrity of the embedded carbon steel bars. One of the primary factors affecting this integrity is the susceptibility of the steel to corrosion, which can cause significant structural deterioration and compromise the safety of these structures. The corrosion resistance of the reinforcing carbon steel bars in concrete depends on the formation of a protective passive layer that forms in the alkaline environment of concrete [1,2]. It is known that this layer is an ultrathin (<10 nm), protective oxide, or hydroxide film that decreases the dissolution rate of steel to negligible levels [3]. Therefore, understanding the mechanisms and kinetics of passive layer formation on steel surfaces is crucial for developing more durable and corrosion-resistant materials. Several studies indicated that the formation of the passive layer is a time-dependent process [4–8].

Pearlite, bainite, and martensite are three important microstructures in carbon steel that form under different cooling conditions. Pearlite consisted of alternating layers of α-ferrite (relatively pure iron with a body-centered-cubic structure) and cementite (iron carbide). Bainite comprises a fine, nonlamellar mixture of α-ferrite and cementite. Martensite contains a distorted iron lattice, forming a body-centered tetragonal crystal structure. The microstructures within the carbon steel can influence the formation of the passive layer since pearlite, bainite, and martensite each exhibit distinct effects on passivation in alkaline solutions. These three microstructures exhibit distinct properties. Thus, the formation of a passive layer on each microstructure can also be different.

A few studies have investigated the influence of microstructure on the passivation. Yilmaz et al. [9] studied the influence of ferrite-martensite and ferrite-pearlite combinations on the formation of the passive layer on low-carbon steel in a 0.1 M NaOH solution. Their study showed that a stronger passive film was formed on the ferrite-pearlite microstructure than on the ferrite-martensite microstructure. Yanagisawa et al. [10] also examined the passivity of dual-phase carbon steel with ferrite and martensite microstructure at a pH of 8.4 in boric acid-borate buffer solution. Their results indicated that the passive layer on the dual microstructure, i.e., martensite +

* Corresponding author.
E-mail address: gdavira@clemson.edu (G. Daviran).

https://doi.org/10.1016/j.mtla.2024.102277
Received 8 September 2024; Accepted 24 October 2024
Available online 24 October 2024
2589-1529/Published by Elsevier B.V. on behalf of Acta Materialia Inc.

ferrite, was stronger with less defects than on the pure martensite microstructure. Hussain and his colleagues investigated the passivation on two types of reinforcing steel bars, one with tempered martensite and the other with ferrite-pearlite microstructures [11]. Their results showed that the passive layer on the surface of steel with tempered martensite microstructure formed at a notably higher rate and was more stable than that on steel with ferrite-pearlite microstructure.

Previous studies indicated that the kinetics of the passive layer's formation on different steel microstructures occur at different rates. Further study of the kinetics of the formation of passive layers on different steel microstructures is required, which is the objective of this work. This research utilized a high-throughput approach using Scanning Electrochemical Microscopy (SECM) to study the formation and kinetics of the passive layer on pearlite, bainite, and martensite microstructures. SECM has emerged as a powerful tool with numerous advantages over conventional methods in various fields. SECM offers high-resolution imaging capabilities in temporal and lateral resolutions [12]. This technique allows for the characterization of processes such as electron transfer, adsorption, and reaction kinetics at the nanoscale level [13]. The time-dependent process of passive layer formation, the passivation kinetics, and the effective rate constant of the species in the solution were evaluated. Thermomechanical treatment can produce steel with a combined microstructure consisting of martensite in the outer layer, bainite in the middle, and pearlite in the center. Due to the presence of all three microstructures in the thermomechanical treatment (TMT) steel, it was used in this study.

1.1. SECM

In SECM, a mediator is used to facilitate the detection of electrochemical activities at the sample surface. It contains redox-active species that transfer electrons between the SECM tip and the sample surface, thus amplifying the electrochemical signals. This process improves the sensitivity of the measurements, making it easier to detect and quantify the reactivity of the sample. When a steel sample is exposed to an alkaline solution, the formation of the passive layer significantly reduces the transfer of electrons. Detecting this very low electrical current by the SECM tip would be nearly impossible without a mediator. This study used the feedback mode of SECM to conduct all subsequent experiments and measurements. Some advantages of feedback mode consist of but are not limited to high spatial resolution, non-destructive analysis, dynamic process monitoring, local corrosion studies, and quantitative information regarding the kinetics of surface reactions [14–16].

The 10 μm diameter ultra microelectrode (UME) with the RG ratio of 10 was used as the scanning probe. The RG ratio is the ratio of the radius of the probe's insulating cover over the electrode's active area. The SECM probe was calibrated using a standard redox couple of ferro/ferricyanide to ensure accurate measurement of the feedback current. Additionally, its functionality was validated against a gold-mounted sample, whose characterization is well-known within the system [17]. Prior to each experiment, the UME was polished smoothly with the 1200# grid sandpaper and rinsed with deionized water. Platinum and Ag/AgCl were used as the counter and reference electrodes, respectively. All measurements were conducted at room temperature.

1.2. Approach curves

An approach curve is a plot that illustrates how the current measured at the UME tip changes as the tip approaches the surface of the sample. The approach curve is an essential tool used to determine the distance between the UME and the surface of the sample and to study the electrochemical activities adjacent to the surface of the sample.

The UME was positioned above the sample and slowly moved down until it touched the surface. It then retracted to +10 μm from the surface. The tip subsequently moved up to a position of +200 μm. During all measurements, the tip was approached at a velocity of 1 μm/s, ensuring stable current acquisition from the SECM. During experiments, a positive voltage of 0.65 V versus Ag/AgCl was applied to the UME tip. No voltage was applied to the sample, allowing for a clear understanding of heterogeneous electron transfer processes [18]. The first approach curve measurement was conducted after 5 min of exposing the sample to the solution and then repeated 5, 24 and 72 h after that. All measurements were repeated three times.

1.3. Line scan

A line scan in SECM is a measurement technique where the UME is moved along a straight line across the surface of the sample, and the electrochemical current is recorded continuously along this line. This technique provides spatially resolved information about the electrochemical activity of the sample along the scanned line. For the line scan test, the UME tip moved with the scan rate of 1 μm/s starting from the martensite region and passing through the bainite and pearlite regions. The line scan measurements were employed with similar intervals as the approach curve experiments. All experiments were repeated three times.

1.4. Cyclic voltammetry

Cyclic voltammetry (CV) in SECM provides detailed information on the electrochemical properties of a sample. By analyzing the CV plots, redox potentials, electron transfer rates, and surface coverage of electroactive sites can be studied [19,20]. CV measurements were conducted on each microstructure region after 5 min, 1, 3, 5, 24 and 72 hours after exposing the surface to the solution to study the kinetics of the formation of the passive layer. Results were used to calculate the diffusion coefficient of electroactive species and estimate the effective rate coefficient, i.e., k_{eff}.

Effective rate coefficient (k_{eff})

k_{eff} indicates the overall reaction rate of the experiments by merging the natural rate constant of an electrochemical reaction with mass transport effects, predominantly diffusion. It captures how effectively reactants reach the electrode surface and contribute to electrochemical reactions [8,21,22]. When the UME approaches the surface, the current sensed by the UME is influenced by the normalized distance value, i.e., the distance/tip diameter, of L. The current at L distance, $I_T(L)$, can be determined as:

$$IT(L) = \left[{I_T}^{ins}(L) + I_S(L)\left(1 - \frac{I_T^{ins}(L)}{I_T^{con}(L)}\right)\right] \quad (1)$$

where $I_S(L)$ is the kinetically controlled substrate current, and $I_T^{con}(L)$ and $I_T^{ins}(L)$ represent the tip currents corresponding to diffusion-controlled regeneration of a redox mediator and an insulating substrate (no mediator regeneration), respectively. For RG ~10, equation 1 can be rewritten as [23]:

$$I_T^{con} = 0.7449932 + \frac{0.7582943}{L} + 0.2353042 \cdot e^{-\frac{1.683087}{L}} \quad (2)$$

$$I_T^{ins}(L) = \frac{1}{0.4571825 + \frac{1.4604238}{L} + 0.4312735 \cdot e^{-\frac{2.350667}{L}}} + \frac{-0.145437 \cdot L}{5.5768952 + L} \quad (3)$$

$I_S(L)$ can be expressed in terms of the normalized first-order rate constant κ as:

$$I_s(L) = \frac{0.78377}{L\left(1 + \frac{1}{\kappa L}\right)} + \frac{0.68 + 0.3315e^{\frac{-1.0672}{L}}}{1 + \frac{\frac{11}{\kappa L} + 7.3}{110 - 40L}} \quad (4)$$

$\frac{I_T^{ins}(L)}{I_T^{con}(L)}$ ratio in equation 1 can be calculated using Eqs. (2) and (3). Furthermore, $I_s(L)$ can be obtained using different values of L and κ. Using the best theoretical approach curve, k_{eff} can be obtained as:

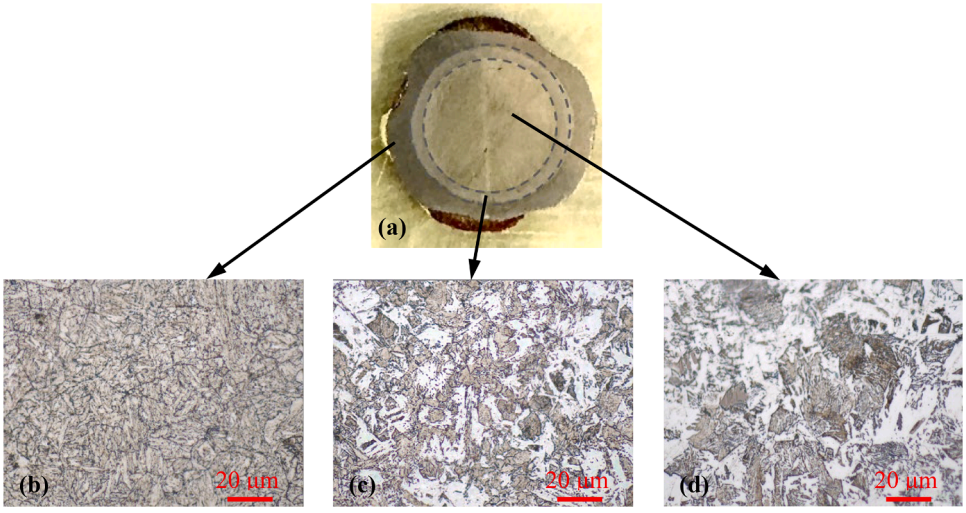

Fig. 1. (a) Cross-sectional image of a TMT bar and the optical microscopic images of (b) tempered martensite phase, (c) bainite, and (d) pearlite microstructures.

Table 1
Composition of concrete simulated pore solution.

Compound	mol/L
KOH	0.3
NaOH	0.1
Ca $(OH)_2$	0.03
CaSO4.2H2O (gypsum)	0.003
K_3 [Fe(CN)6] (Mediator)	0.0005

$$k_{eff} = \kappa \cdot \frac{D}{r} \quad (5)$$

where D is the diffusion coefficient of the mediator and r is the UME tip radius.

To measure the diffusion coefficient of potassium ferrocyanide in a simulated concrete pore solution, the Randles-Sevcik [24] equation was used. This equation predicts the peak current, i_p, as a function of the sweep rate (ν) as:

$$i_p = 0.446nFCA\sqrt{\frac{nF\nu D}{RT}} \quad (6)$$

In Eq. (6), n is the number of electrons involved in redox reaction ($Fe(CN)_6^{3-} + 1e^- \leftrightarrow Fe(CN)_6^{4-}$), F is Faraday constant (96500 C. mol^{-1}), C represents the concentration of the electroactive species (0.5 mM, in this study), A is the surface area of the working electrode (113.1 mm^2 in this case), T indicates the temperature (the experiment was conducted at ambient temperature, i.e., 297K), R denotes for the gas constant, and D is the diffusion coefficient.

2. Experimental procedures

2.1. Materials

Thermomechanically treated (TMT) carbon steel bars with the chemical composition of 0.310% C, 1.230% Mn, 0.018% P, 0.024% S, 0.290% Si, 0.230% Cu, 0.080% Ni, 0.016% Mo, 0.002% V, and 97.8% Fe were used in this study. The TMT steel has three distinct microstructures, including tempered martensite, bainite, and pearlite, as shown in Fig. 1. The features and separate microstructure within the bar cross-section were ideal for investigating the passivation across different microstructures.

Three identical samples were used for each test. Steel samples were cut to the length of 10 mm from a TMT bar and mounted using two-part cold epoxy at room temperature. The samples were progressively grounded using SiC sandpaper with 240#, 400#, 600#, 800#, and 1200# grids; then, they were polished using 1µm alumina slurry. For each test, a mounted steel sample was embedded in the SECM sample holder, which allowed the solution to be poured on top of the sample. The solution with the composition in Table 1 was used for all experiments. This solution comprised the compounds used in simulated concrete pore solution [7], plus potassium ferricyanide ($K_3[Fe(CN)_6]$) as the mediator. Samples were immersed in the solution for three days to ascertain the formation of the passive layer [7,25].

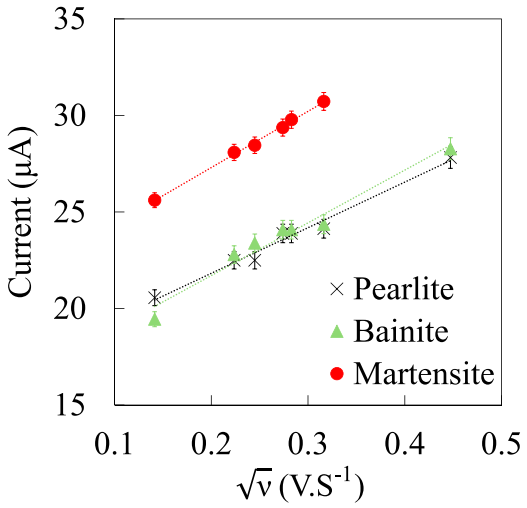

Fig. 2. The anodic peak values from CV tests for 0.5 mM potassium ferrocyanide in simulated concrete pore solution as a function of the square root of the scan rate for different microstructures.

3. Results and discussion

CV experiments with scan rates of 20, 50, 75, 80, 100 and 200 mV/s were conducted on each microstructure. The anodic peaks from each voltammogram were used to plot i_p versus $\sqrt{\nu}$ plots; these are shown in Fig. 2. D, the slope of the plot, was determined as 6.81×10^{-7}, 4.48×10^{-7}, and 4.37×10^{-7} cm^2s^{-1} for martensite, bainite, and pearlite, respectively, with certainty of more than 92% based on the least square method.

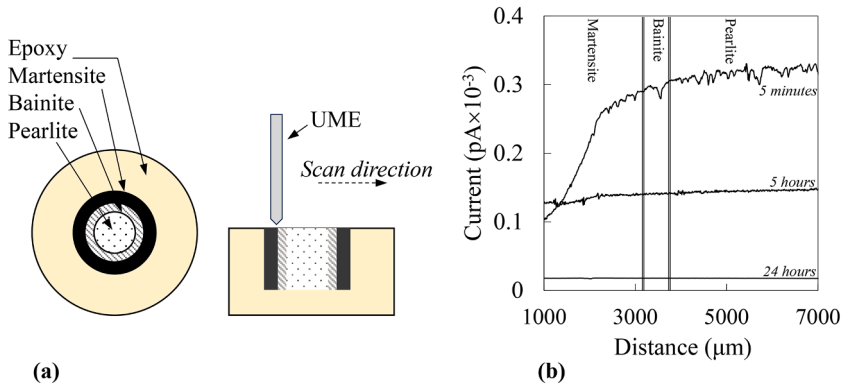

Fig. 3. (a) schematic illustration of a sample and the scanning (b) Line scans of a sample over different exposure times in the solution.

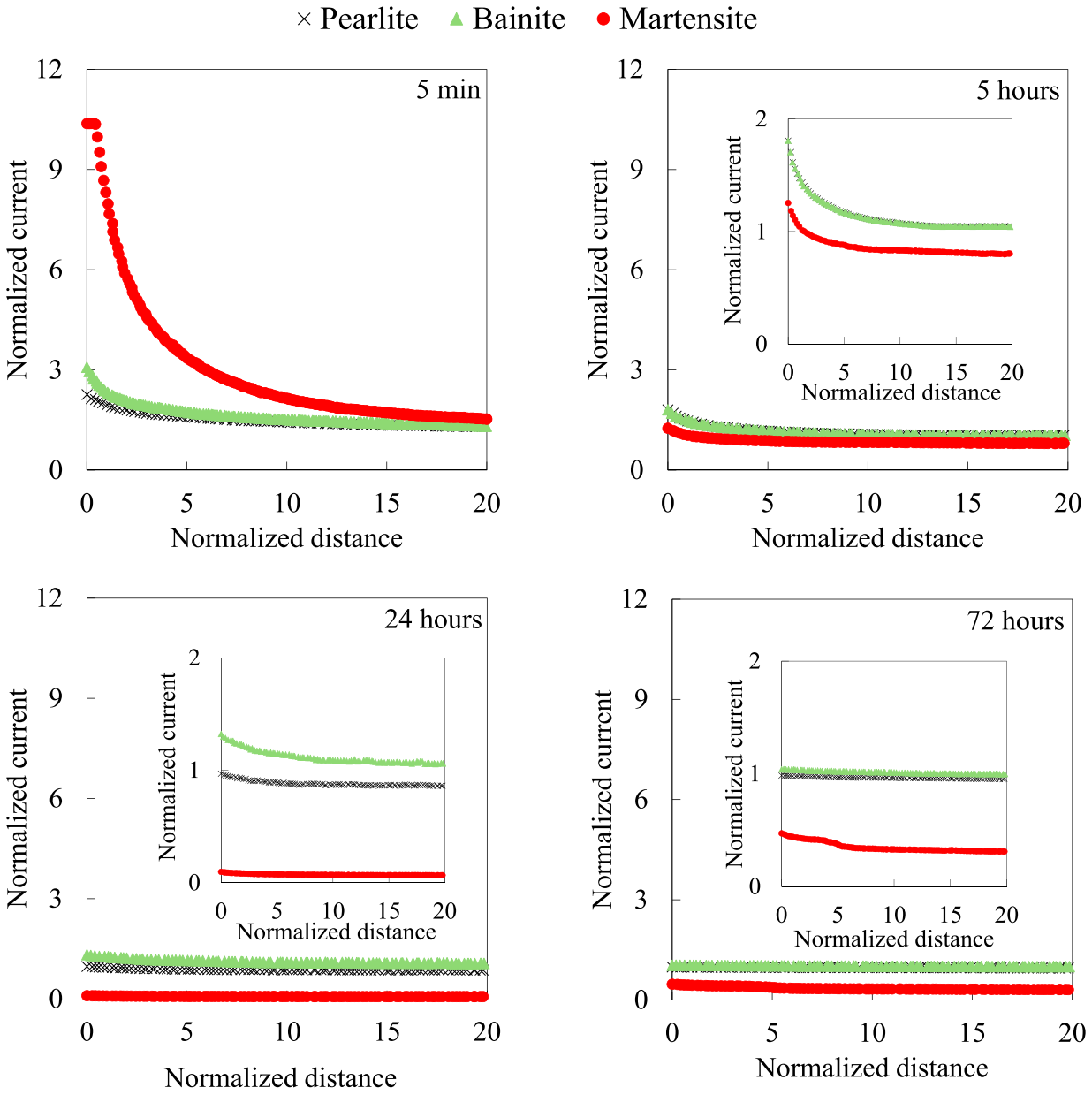

Fig. 4. Approach curves for different microstructures within a sample immersed in the test solution at different times after exposure.

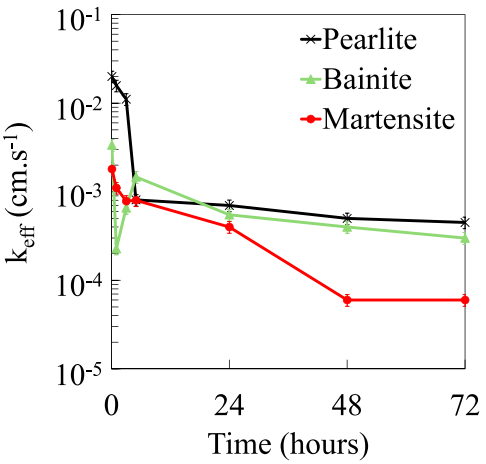

Fig. 5. Calculated k_{eff} at different times after exposure of a sample in the solution.

3.1. Kinetics of the formation of the passive layer

Fig. 3 shows the results of the line scan test on a sample at different times after immersion in the solution. Line scans began above the martensite microstructure, continued through the bainite and pearlite microstructures, respectively, and stopped in the middle of the sample. A few minutes after exposing the sample to the solution, samples showed higher currents, regardless of the microstructure. As time passed, the current decreased, indicating the formation of the passive layer on all microstructures. The exception occurred at the beginning of the exposure, i.e., at 5 min, no significant change in current values was observed on the different microstructures. This observation can be attributed to extremely low current (pico Amp) beyond the system's sensitivity.

Fig. 4 shows the approach curves of a sample at different times after exposure to the solution. In Fig. 4, the X-axes are the normalized distance, which is the ratio of the distance of the UME tip to the surface of the sample and the radius of the active area of the UME electrode. The Y-axes show the normalized current, i.e., the ratio of the oxidation current, recorded from near the surface, to the infinite current, recorded from the bulk of the solution.

Results indicated that within a few minutes after immersion of the sample in the solution, electron transfer occurred rapidly between iron ions and the solution active species, and the steel surface acted as a pure conductive surface [26,27]. However, after a few hours, the passive layer started to form on the surface of all microstructures, leading to a decrease in the tip current. Except for the beginning of the immersion, i.e., 5 min, the martensite phase indicated a lower current than the pearlite and bainite phases. This difference increased by increasing the exposure time, showing the superior passive layer on martensite compared to the other microstructures. To better understand the kinetics of passivation over different microstructures, the k_{eff} was calculated for all microstructures, and the results are summarized in Fig. 5.

A notable decrease in the k_{eff} value was observed immediately after exposure to the solution. This observation was ascribed to the fact that the steel surface, regardless of the microstructure, was kinetically active at the beginning of the exposure. Therefore, the electron transfer occurred quickly between the steel surface and the ions in the solution. During the formation of a passive layer on the surface of steel in concrete pore solution, the ratio of Fe^{2+}/Fe^{3+} increases through the whole depth of the passive layer [28,29]. Consequently, it was hypothesized that within a few minutes after exposure to the solution, the UME constantly collected current from the steel surface due to the release of the electrons from the $Fe \rightarrow Fe^{2+} + 2e^-$ reaction. With time, the passive layer grew, and the k_{eff} decreased. $Fe^{2+} \rightarrow Fe^{3+} + e^-$ became the prevalent oxidation reaction between the solution and the steel sample. The decrease in the k_{eff} value can be attributed to a decrease in the number of released electrons, i.e., 2 to 1 for each iron ion. The outward flux of Fe^{2+} was more than the diffusivity of O^{2-}. Thus, simultaneously, the oxygen vacancies were generated at the interface of the steel sample and the passive layer [30]. As a result, as time progressed, the donor density of the passive layer decreased [31], and the k_{eff} values moved toward a relatively steady state, indicating the complete formation of the passive layer.

When the passive layers were not stable at the beginning of the test, fluctuations were observed in the k_{eff} values. Twenty-four hours after exposure, however, the value became more stable. While the k_{eff} values for the pearlite and bainite microstructures were comparable, the martensite showed considerably lower k_{eff} values than the pearlite and bainite. These results agree with the approach curve test results, i.e., the integrity of the passive film on the martensite was superior to the other phases.

Results from both approach curves and k_{eff} showed that the martensite had a more active surface than pearlite and bainite. This activity led to the formation of a more rapid and stable passive layer on martensite compared to the other microstructures. It was hypothesized that several factors could potentially explain this observation. As shown in Fig. 1b, martensite has an entangled and complex microstructure with finer grains than bainite, Fig. 1c, and pearlite, Fig. 1d. Both pearlite and bainite had distinct cementite and ferrite phases in their microstructure. Cementite can act as the site for cathodic reactions in the microgalvanic cell formed between the ferritic and cementite phases [32]. However, in the much more complex microstructure of martensite, the anodic and cathodic reactions had a more difficult time to occur. As a result, the overall corrosion rate, i.e., current, on the martensite was lower than that on pearlite and bainite. Additionally, their microstructural features led to a relativity similar passive layer on both pearlite and bainite.

4. Conclusions

It can be concluded that:

- SECM provided valuable insights into the reaction kinetics and spatial distribution of passivation across the heterogeneous microstructure of the steel sample.
- Forming the passive layer is a time-dependent process. The kinetic activities were initiated shortly after exposing the steel sample to a simulated concrete pore solution with the mediator. However, after one hour, the passive layer began to form on the surface of each microstructure and remained stable.
- The passivation in steel samples was influenced by its microstructure. Martensite demonstrated superior passivation behavior compared to pearlite and bainite, probably due to its complex features. It is hypothesized that the formation of galvanic coupling between ferrite and cementite in pearlite and bainite is responsible for the inferior passive film on these two microstructures compared to martensite. Nonetheless, this hypothesis requires further investigation.
- Understanding these relationships between microstructure and passivation behavior is crucial for developing more corrosion-resistant steel for reinforced concrete structures. The insights gained from this study can guide the optimization of steel microstructure with enhanced durability and safety.
- It should be noted that the objective of this study was to use a high-throughput approach to examine the kinetics of the formation of the passive layers on different microstructures. While the results indicated that the passive layer formed faster, which probably was more stable on the martensite than the pearlite and bainite, the integrity of that layer is not studied in this work.

CRediT authorship contribution statement

Gisoo Daviran: Writing – review & editing, Writing – original draft, Validation. **S. M. Ali Seyed Mahmoud:** Writing – review & editing, Writing – original draft. **Surya R. Kalidindi:** Writing – review & editing, Writing – original draft. **Amir Poursaee:** Writing – review & editing, Writing – original draft, Supervision.

Declaration of competing interest

I declare that I have no known competing financial interests or personal relationships that could have appeared to influence the work reported in this article

Acknowledgment

This work was conducted in the Corrosion Research Laboratory (CorRLab) at Clemson University. This study is funded by National Science Foundation Grant Nos. 2221098 and 2221104, which is greatly acknowledged. Any opinions, findings, conclusions, or recommendations expressed in this material are those of the authors and do not necessarily reflect the views of the National Science Foundation.

References

[1] B. Elsener, Macrocell corrosion of steel in concrete – implications for corrosion monitoring, Cem. Concr. Compos. 24 (1) (2002) 65–72, https://doi.org/10.1016/S0958-9465(01)00027-0.
[2] P. Garcés, M.C. Andrade, A. Saez, M.C. Alonso, Corrosion of reinforcing steel in neutral and acid solutions simulating the electrolytic environments in the micropores of concrete in the propagation period, Corros. Sci. 47 (2) (2005) 289–306, https://doi.org/10.1016/j.corsci.2004.06.004.
[3] A. Poursaee, U.M. Angst, Principles of corrosion of steel in concrete structures, Corros. Steel Concr. Struct. (2023) 17–34, https://doi.org/10.1016/B978-0-12-821840-2.00004-3. Elsevier.
[4] C.A. Sequeira, D.M. Santos, J.R. Sousa, P. Brito, The mechanism of oxide film formation on AISI 316 stainless steel in sulphate solutions, ECS Trans. 16 (48) (2009) 67–77, https://doi.org/10.1149/1.3149570.
[5] Y. Han, Z.D. Cui, Q. Wei, S.L. Zhu, X.J. Yang, Kinetics of passive film on low carbon steel in sodium nitrate solution by numerical analysis method, Adv. Mater. Res. 457–458 (2012) 358–364, https://doi.org/10.4028/www.scientific.net/AMR.457-458.358.
[6] R.S. Lillard, G. Vasquez, D.F. Bahr, The kinetics of anodic dissolution and repassivation on stainless steel 304L in solutions containing nitrate, J. Electrochem. Soc. 158 (6) (2011) C194, https://doi.org/10.1149/1.3574367.
[7] A. Poursaee, C.M. Hansson, Reinforcing steel passivation in mortar and pore solution, Cem. Concr. Res. 37 (7) (2007) 1127–1133, https://doi.org/10.1016/j.cemconres.2007.04.005.
[8] H. Torbati-Sarraf, A. Poursaee, Study of the passivation of carbon steel in simulated concrete pore solution using scanning electrochemical microscope (SECM), Materialia 2 (2018) 19–22, https://doi.org/10.1016/j.mtla.2018.08.011 (Oxf).
[9] A. Yilmaz, C. Ozkan, J. Sietsma, Y. Gonzalez-Garcia, Properties of passive films formed on ferrite-martensite and ferrite-pearlite steel microstructures, Metals 11 (4) (2021), https://doi.org/10.3390/met11040594 (Basel).
[10] K. Yanagisawa, T. Nakanishi, Y. Hasegawa, K. Fushimi, Passivity of dual-phase carbon steel with ferrite and martensite phases in pH 8.4 boric acid-borate buffer solution, J. Electrochem. Soc. 162 (7) (2015) C322–C326, https://doi.org/10.1149/2.0471507jes.
[11] R.R. Hussain, et al., Effect of reinforcing bar microstructure on passive film exposed to simulated concrete pore solution, ACI Mater. J. 115 (2) (2018), https://doi.org/10.14359/51701237.
[12] A.J. Bard, F.R.F. Fan, Juhyoun. Kwak, and Ovadia. Lev, Scanning electrochemical microscopy. Introduction and principles, Anal. Chem. 61 (2) (1989) 132–138, https://doi.org/10.1021/ac00177a011.
[13] C.H. Ryu, Y. Nam, H.S. Ahn, Modern Applications of scanning electrochemical microscopy in the analysis of electrocatalytic surface reactions, Chin. J. Catal. 43 (1) (2022) 59–70, https://doi.org/10.1016/S1872-2067(21)63948-7.
[14] Q. Zhou, Y. Wang, D.E. Tallman, M.B. Jensen, Simulation of SECM approach curves for heterogeneous metal surfaces, J. Electrochem. Soc. 159 (7) (2012) H644–H649, https://doi.org/10.1149/2.034207jes.
[15] P. Dauphin-Ducharme, et al., Local hydrogen fluxes correlated to microstructural features of a corroding sand cast AM50 magnesium alloy, J. Electrochem. Soc. 161 (12) (2014) C557–C564, https://doi.org/10.1149/2.0571412jes.
[16] M.A. Malik, P.J. Kulesza, Monitoring of conductivity changes in passive layers by scanning electrochemical microscopy in feedback mode: localization of pitting precursor sites on surfaces of multimetallic phase materials, Anal. Chem. 79 (11) (2007) 3996–4005, https://doi.org/10.1021/ac061664f.
[17] C. Wei, A.J. Bard, M.V. Mirkin, Scanning electrochemical microscopy. 31. Application of SECM to the study of charge transfer processes at the liquid/liquid interface, J. Phys. Chem. 99 (43) (1995) 16033–16042, https://doi.org/10.1021/j100043a050.
[18] H. Xiong, J. Guo, S. Amemiya, Probing heterogeneous electron transfer at an unbiased conductor by scanning electrochemical microscopy in the feedback mode, Anal. Chem. 79 (7) (2007) 2735–2744, https://doi.org/10.1021/ac062089i.
[19] D.S. Schrock, J.E. Baur, Chemical imaging with combined fast-scan cyclic voltammetry−scanning electrochemical microscopy, Anal. Chem. 79 (18) (2007) 7053–7061, https://doi.org/10.1021/ac071155t.
[20] C. Cannes, F. Kanoufi, A.J. Bard, Cyclic voltammetry and scanning electrochemical microscopy of ferrocenemethanol at monolayer and bilayer-modified gold electrodes, J. Electroanal. Chem. 547 (1) (2003) 83–91, https://doi.org/10.1016/S0022-0728(03)00192-X.
[21] C. Wei, A.J. Bard, M.V. Mirkin, Scanning electrochemical microscopy. 31. Application of SECM to the study of charge transfer processes at the liquid/liquid interface, J. Phys. Chem. 99 (43) (1995) 16033–16042, https://doi.org/10.1021/j100043a050.
[22] A. Asserghine, D. Filotás, L. Nagy, G. Nagy, Scanning electrochemical microscopy investigation of the rate of formation of a passivating TiO 2 layer on a Ti G4 dental implant, Electrochem. Commun. 83 (2017) 33–35, https://doi.org/10.1016/j.elecom.2017.08.018.
[23] Y. Shao, M.V. Mirkin, Probing ion transfer at the liquid/liquid interface by scanning electrochemical microscopy (SECM), J. Phys. Chem. B 102 (49) (1998) 9915–9921, https://doi.org/10.1021/jp9828282.
[24] K. Ngamchuea, S. Eloul, K. Tschulik, R.G. Compton, Planar diffusion to macro disc electrodes—what electrode size is required for the cottrell and randles-sevcik equations to apply quantitatively? J. Solid State Electrochem. 18 (12) (2014) 3251–3257, https://doi.org/10.1007/s10008-014-2664-z.
[25] S. Reza Allahkaram, M. Khodayari, Electrochemical noise analysis of carbon steel in simulated concrete pore solution affected by CO_2 and SO_2 using wavelet transform, Anti-Corros. Methods Mater. 55 (5) (2008) 250–256, https://doi.org/10.1108/00035590810903836.
[26] M.A. Climent, C. Gutiérrez, Proof by UV-visible modulated reflectance spectroscopy of the breakdown by carbonation of the passivating layer on iron in alkaline solution, Surf. Sci. 330 (1) (1995) L651–L656, https://doi.org/10.1016/0039-6028(95)00429-7.
[27] B. Huet, V. L'Hostis, F. Miserque, H. Idrissi, Electrochemical behavior of mild steel in concrete: influence of pH and carbonate content of concrete pore solution, Electrochim. Acta 51 (1) (2005) 172–180, https://doi.org/10.1016/j.electacta.2005.04.014.
[28] H.B. Gunay, P. Ghods, O.B. Isgor, G.J.C. Carpenter, X. Wu, Characterization of atomic structure of oxide films on carbon steel in simulated concrete pore solutions using EELS, Appl. Surf. Sci. 274 (2013) 195–202, https://doi.org/10.1016/j.apsusc.2013.03.014.
[29] C.G. Zoski, M.V. Mirkin, Steady-state limiting currents at finite conical microelectrodes, Anal. Chem. 74 (9) (2002) 1986–1992, https://doi.org/10.1021/ac015669i.
[30] Z.H. Dong, W. Shi, G.A. Zhang, X.P. Guo, The role of inhibitors on the repassivation of pitting corrosion of carbon steel in synthetic carbonated concrete pore solution, Electrochim. Acta 56 (17) (2011) 5890–5897, https://doi.org/10.1016/j.electacta.2011.04.120.
[31] A. Poursaee, Temperature dependence of the formation of the passivation layer on carbon steel in high alkaline environment of concrete pore solution, Electrochem. Commun. 73 (2016) 24–28, https://doi.org/10.1016/j.elecom.2016.10.003.
[32] P.K. Katiyar, S. Misra, K. Mondal, Comparative corrosion behavior of five microstructures (Pearlite, Bainite, Spheroidized, Martensite, and Tempered Martensite) Made from a high carbon steel, Metall. Mater. Trans. A 50 (3) (2019) 1489–1501, https://doi.org/10.1007/s11661-018-5086-1.